Biological and Environmental Phenomena at the Interface

Membrane stability in the presence of methacrylate esters

Vivien Yeh, Alice Goode, Graham Eastham, Robert Rambo, Katsuaki Inoue, James J. Doutch, and Boyan B Bonev

Langmuir, **Just Accepted Manuscript** • DOI: 10.1021/acs.langmuir.9b03759 • Publication Date (Web): 23 Mar 2020

Membrane stability in the presence of methacrylate esters

Vivien Yeh[1], Alice Goode[1], Graham Eastham[2], Robert P. Rambo[3], Katsuaki Inoue[3], James Doutch[4], Boyan B. Bonev[1*]

[1] School of Life Sciences, University of Nottingham, Nottingham, NG7 2UH, UK

[2] Lucite International, Wilton Centre, Wilton, Redcar, UK

[3] Diamond Light Source, Harwell Science & Innovation Campus, Didcot, OX11 0DE, UK

[4] Science and Technology Facilities Council, ISIS Neutron and Muon Source, Rutherford Appleton Laboratory, Didcot, OX11 0QX, UK

[*] Corresponding author

KEYWORDS

Lipid membranes, membrane phase stability, methacrylate esters, solid state NMR, SAXS

Abbreviations: DOPC –1,2-dioleoyl-*sn*-glycero-3-phosphocholine; DMPC – 1,2-dimyristoyl-sn-glycero-3-phosphocholine; DPPC – 1,2-dipalmitoyl-*sn*-glycero-3-phosphocholine; POPC – 1-palmitoyl-2-oleoyl-glycero-3-phosphocholine; DEPC – 1,2-dielaidoyl-*sn*-glycero-3-phosphocholine; BMA – *n*-butyl methacrylate, NMR – nuclear magnetic resonance; MAS- magic angle sample spinning; SAXS – small angle X-ray scattering;

Correspondence email: boyan.bonev@nottingham.ac.uk

ABSTRACT

Bioproduction of polymethyl methacrylate is a fast growing global industry that is limited by cellular toxicity of monomeric methacrylate intermediates to the producer strains. Maintaining high methacrylate concentrations during biofermentation, required by economically viable technologies, challenges bacterial membrane stability and cellular viability. Studying the stability of model lipid membranes in the presence of methacrylates offers unique molecular insights into the mechanisms of methacrylate toxicity, as well as into the fundamental structural bases of membrane assembly. We investigate the structure and stability of model membranes in the presence of high levels of methacrylate esters using solid-state nuclear magnetic resonance (NMR) and small angle X-ray scattering (SAXS). Wideline ^{31}P NMR spectroscopy shows that butyl methacrylate (BMA) can be incorporated into the lipid bilayer at concentrations as high as 75 mol% without significantly disrupting membrane integrity and that lipid acyl chain composition can influence membrane tolerance and ability to accommodate BMA. Using high resolution ^{13}C magic angle spinning (MAS) NMR we show that the presence of 75 mol% BMA lowers the lipid main transition temperature by over 12 degrees, which suggests BMA intercalates between the lipid chains causing uncoupling of collective lipid motions that are typically dominated by chain *trans-gauche* isomerisation. Potential uncoupling of the bilayer leaflets to accommodate a separate BMA sub-phase was not supported by the SAXS experiments, which showed that membrane thickness remained unchanged even at 80% BMA. Reduced X-ray scattering contrast at the polar/apolar interface suggests BMA localisation in that region between the lipid molecules.

INTRODUCTION

Polymethyl methacrylate, PMMA, is a clear lightweight plastic and one of the most widely used polymer materials in the world with a global market of around $4.6 bn estimated to reach $6.66 bn by 2026[1]. Petrochemicals are the major feedstock for industrial production of PMMA. In favour of more sustainable production of PMMA precursors, bio-production of monomeric methacrylate ester (MAE) by fermentation is an area of research and development by the world's leading manufacturer of methacrylate esters, Mitsubishi Chemical Corporation. Biotechnological approaches such as metabolic pathway development and strain and construct design, have shown promising potential in manufacturing a wide range of chemicals from sustainable feedstock[2,3]. However, unlike naturally occurring metabolic products like succinic acid and lactic acid, where either compound can be produced on the scale of 100g per litre by *Escherichia coli*[4,5], production of monomeric MAE leads to problematic cytotoxicity, particularly as the concentration of product builds up and accumulates in the organism. In that regard, understanding the product interactions with host cell membranes and obtaining guidelines for engineering product-tolerant membranes is an essential component in the process development through improving strain performance and efficiency.

Maintaining cell membrane integrity in high MAE levels is key to improving cell viability and membrane damage is a prime mechanism of product toxicity[6–8]. During biofermentative production MAE concentrations in bioreactors increase to levels (IC50 values for *E. coli* and *S. cerevisiae* ranging from 0.09g/l for butyl methacrylate to 3.7g/l for methyl methacrylate[9]) capable of interfering with membrane function and stability, which results in stationary and

declining populations that seriously limit the productivity of engineered strains and product yields.

Gram-negative biofermentation systems, such as *E. coli* and *Pseudomonas putida*, have both a plasma membrane and an outer membrane. The inner, plasma membrane, is largely made of phospholipids and helical transmembrane domain membrane proteins, while the outer membrane is an asymmetric bilayer with phospholipid inner leaflet, an outer leaflet almost entirely made of lipopolysaccharide, LPS,[10] and contains β-barrel membrane proteins. The inner membrane is responsible for maintaining cell viability through protonomotive force (PMF), solute and other physiologically important gradients. The outer membrane provides a periplasmic compartment that plays biologically important roles including post-translational modification of proteins, as well as protecting the cells from xenobiotics and mediating cellular interactions. Both membranes must be intact and functional in order to maintain a healthy and productive fermentative culture.

The principal lipid constituents of the inner membrane and the inner leaflet of the outer membrane in *E. coli* are 72-80% phosphatidylethanolamine (PE), 21-17% phosphatidylglycerol (PG) and 4-7% diphosphatidylglycerol (cardiolipin)[11,12]. The acyl chain composition depends on environmental factors, such as temperature. While it is less readily described, it is generally accepted that at 37°C *E. coli* membrane lipid composition includes 50/45% saturated/unsaturated lipids primarily of C16:0 (45%), C18:1 Δ 11 (30%) and C16:1 Δ 9 (15%)[11]. Mixed chain phospholipids commonly have a saturated acyl chain in glycerol

position *sn*-1' and an unsaturated chain in *sn*-2'. Increase in chain saturation and hydrophobic length has been reported as an adaptive response to hydrocarbon solvents in *P. putida*[13,14].

Biofermentative production of apolar organic solvents is challenging and molecular hydrophobicity is an important determinant of chemical toxicity to membranes. Solvents with low partition coefficient, *Log P,* values are generally non-toxic to membranes[14,15], while *Log P* values within 1.5 – 4 readily partition into membranes[16] and show membrane toxicity[13]. Bacterial adaptations to alkanols of chain length near the lower end of the range include decrease in chain length, while towards the higher end the trend is reversed[17,18].

Some effects of organic solvents on bacterial membrane have been previously studied[13]. For example, toluene has a *Log P* value of 2.5 and has been reported to disrupt the inner membranes of Gram-negative bacteria by converting membranes into inverted hexagonal, H_{II}, phases[19] with associated loss of cytoplasmic proteins and ions, lipids and dissipation of membrane potentials, ultimately leading to cell death[20–22].

Butyl methacrylate, BMA, is a potential intermediate in the production of methyl methacrylate by biofermentation in a process patented by Lucite International[9] and has a *Log P* value of 2.88[23], which places it within the range of solvents with membrane toxicity. A process producing BMA, which has a water solubility at 25 °C of 0.8g/l[24], allows phase separation for easy separation of the reaction product at low concentration. Achieving such high concentrations of BMA in a fermentation environment presents major challenges to the

plasma membrane stability and viability of the biofermentative organisms.

Challenges to lipid membranes in the presence of high levels of solvents are often answered by a phase conversion from bilayer to a non-bilayer phase to better accommodate the mismatch between headgroup area and the increased apolar chain volume. Limited membrane instability during membrane perturbation leads to phase conversion from bilayer to isotropic or inverted hexagonal phases, usually observed as coexistence of bilayer and non-bilayer phases. Such changes are readily monitored and quantified by following molecular mobility of phospholipid phosphates using ^{31}P nuclear magnetic resonance, NMR[25–27]. Changes in bilayer thickness and lipid phase conversion can also be studied by small angle X ray scattering, SAXS[28].

Incorporation of additional molecular components into membranes can also lead to adaptive changes in bilayer order and organization that are reflected in the main transition temperature, T_m, between the liquid crystalline, L_α, and the tilted lamellar, $P_{\beta'}$ gel phase. As such, changes in T_m reflect changes in chain packing and membrane fluidity and can modulate membrane transport and cell viability. The main transition temperature is governed by contributions from chain *trans-gauche* isomerization and cooperative chain-chain intermolecular interactions[14,29]. At a cellular level, bacteria exposed to organic solvents respond by adjusting the lipid composition of the membrane to mitigate solvent-induced stress from changes in membrane fluidity and order[30,31]. Short-term responses include increasing rigidity of the membrane by changing *cis*-unsaturated to cyclopropyl fatty acids[30], *cis-trans* isomerization of

double bonds[22,32] and altering the fatty acid chain length[30]. Long-term adaptations include altering the ratio of the phospholipid head groups[14] and increased cardiolipin production[30], modification of lipopolysaccharides[33] and production of stress response proteins to improve tolerance and survival[30,34,35].

In this study we investigate the effect of butyl methacrylate on lipid membrane structural integrity and chain dynamics. We hypothesise that hydrophobic methacrylates, such as BMA, partition into lipid bilayers near the membrane interface affecting lipid dynamics and phase stability, and that chain composition – lipid chain length, saturation and *cis*-*trans* isomerization – is an important determinant of membrane stability. We use ^{31}P wideline NMR, to assess bilayer phase integrity and high resolution magic angle spinning, MAS, ^{13}C NMR to monitor changes in chain dynamics and to follow changes segmental molecular dynamics with temperature. We build a model for MAE incorporation into membranes and test model membranes' response to MAE and their ability to accommodate high levels of MAE using solid state NMR and SAXS.

EXPERIMENAL METHODS

Preparation of multilamellar vesicles

Natural abundance ^{13}C DOPC (1,2-dioleoyl-*sn*-glycero-3-phosphocholine), DMPC (1,2-dimyristoyl-sn-glycero-3-phosphocholine), DPPC (1,2-dipalmitoyl-*sn*-glycero-3-phosphocholine), POPC (1-palmitoyl-2-oleoyl-glycero-3-phosphocholine) and DEPC

(1,2-dielaidoyl-*sn*-glycero-3-phosphocholine) were purchased from Avanti Polar Lipids (AL, USA) at >98% purity and used without further purification. Butyl methacrylate was provided by Tokyo Chemical Industry at >99% purity and used without further treatments. In all experiments BMA was added at the desired molar ratio to 20 μmol of lipid powder and mixed for 5 min with a fine glass rod. The sample was then suspended in 500 μl of HPLC grade water and stirred for a further 5 min, then another 500 μl of water were added, mixed and freeze-thawed five times between –196°C and 50°C. Multilamellar vesicles, MLV, obtained in this way were centrifugated at 16,060 ×g (Biofuge *pico*) for 20 minutes at room temperature and the hydrated pellet was loaded into a 4 mm ZrO MAS NMR rotor. MLV suspensions were prepared in the same way for SAXS at 5 mM concentration and were not pelleted. Large unilamellar vesicles, LUVs, were also prepared for SAXS by extrusion of the MLV suspensions through a 100 nm polycarbonate filter using a manual syringe extruder (Avanti Polar Lipids), previously described[10,36].

Solid state NMR

All solid state NMR experiments were performed on Varian 400 MHz VNMRS spectrometer equipped with a 4 mm MAS NMR probe. Temperature was regulated using balanced heated/vortex tube-cooled gas flow, and the measured values were corrected for known heating due to MAS and RF[37,38]. All ^{31}P spectra were referenced externally to 10% H_3PO_4 at 0 ppm, and ^{13}C spectra were referenced externally to adamantine CH_2 at 37.54 ppm. Phosphorus-31 wideline NMR was carried out at a frequency of 161.82 MHz and at a temperature of either 20 °C for DOPC, POPC and DEPC, 28 °C for DMPC or 42 °C for

DPPC using the Hahn echo sequence with 100 kHz π/2 and π-pulses separated by 12 μs interpulse and pre-acquisition delays. Spectra were acquired with 25 ms acquisition time with a recycle delay of 5 s, and with 1024 transients averaged to obtain each FID and processed with 100 Hz Lorentzian line broadening. High resolution ^{13}C CP MAS NMR was done at MAS frequency 5 kHz. The 120 kHz ^{1}H excitation pulse was followed by 3.5 ms of 45 kHz Harmann-Hahn contact for magnetization transfer to ^{13}C. Spectra were acquired under 60 kHz SPINAL-64[39] decoupling scheme over 125 ms and by averaging 1024 transients per FID or under 109 kHz frequency switching Lee-Goldberg (FSLG) decoupling[40] over 75 ms and by averaging 8192 transients, respectively. The recycle delay was set to 3.5s to exceed five times proton T_1 (~0.5s) and all spectra were processed with 2 Hz Lorentzian line broadening.

SAXS

Liposome samples were prepared in a 96-well plate and delivered to the X-ray beam using the Arinax BioSAXS automated liquid handling robot. The sample environment for X-ray exposure, consists of a 1.6 mm diameter, 10 micron thick quartz capillary held in vacuum at 30°C. A detergent wash, water rinse, and flowed air dry cycle was implemented between each measurement. For each sample, a measurement consisted of 30 uL that was flowed through the capillary and a series of 1-second image frames were taken for a total of 30 seconds using an in-vacuum Eiger 4M detector. The X-ray beam measured 800 microns squared at a photon flux of 2x1012 photons per second with the detector at 2.4 meters from the sample position yielding a scattering vector, q, range of 0.012 Å−1< 0.4 Å−1 where q is $4\pi.\sin\theta/\lambda$, 2θ is the scattering angle and λ is the wavelength in Å. 2-D data reduction,

normalisation and integration was performed using DAWN and an in-house Python-based processing pipeline examined and merges the frames into a single 1D curve excluding frames that demonstrated radiation damage or other anomalies.

RESULTS AND DISCUSSIONS

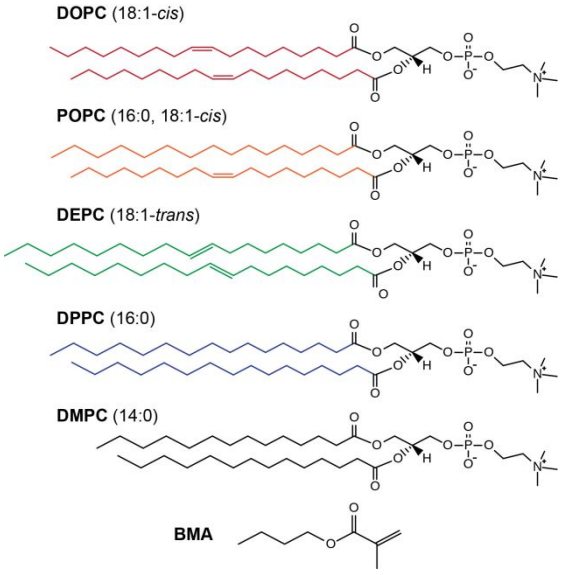

***Figure 1**. Chemical structures of DOPC, POPC, DEPC, DPPC and DMPC showing differences in the lipid chains alongside the structure of BMA.*

To investigate the effects of lipid chain length, saturation and *cis-trans* isomerization on membrane tolerance to BMA we constructed stable, charge-neutral phosphatidylcholine, PC, liposomes of different lipid chain composition. This was done instead of using PE/PG mixtures that mimic better bacterial lipid headgroup composition, due to the intrinsic phase instability of unsupported PE/PG membranes. The use of PC provides a phase-stable reference platform lacking specific binding epitopes, which highlights chain-specific differences in membrane response to BMA. Figure 1 shows the structures of lipids with different chain composition alongside the structure of BMA.

Membrane stability – wideline ^{31}P NMR

Membrane stability in the presence of different BMA concentrations, BMA/DOPC mixtures at molar ratios from 1:2 (33% BMA) to 4:1 (80% BMA), was studied by ^{31}P NMR. Wideline ^{31}P spectra are dominated by motion-averaged, effective chemical shift anisotropy (CSA), which is sensitive to headgroup orientation and local lipid dynamics[41]. The ^{31}P NMR spectra of DOPC liposomes in the presence of BMA are shown in Figure 2 and sample composition is summarised in Table S1. NMR spectra were recorded at 20°C in the liquid crystalline phase, above the main transition temperature of DOPC (−17 °C)[42]. The ^{31}P NMR spectrum of hydrated pure DOPC in Figure 2 is characterized by a powder, Pake, distribution of 45 ppm approximate width, revealing that DOPC is in the liquid crystalline, L_α, phase.

In the presence of increasing concentrations of BMA the powder pattern continues to dominate the ^{31}P spectra, indicating the persistence of the fluid bilayer phase even at 80 molar % BMA. At 75 molar% BMA (3:1 BMA to lipid), a hint of isotropic contribution to the Pake pattern emerged at the isotropic chemical shift of PC of −1 ppm. At 80%mol (4:1 BMA to lipid ratio) BMA, a small isotropic peak at around −1 ppm can be observed. The presence of this isotropic feature reveals the onset of a small contribution from non-bilayer lipid structures with rapid random reorientation dynamics, which reflects marginal instability of bilayer phase. The non-bilayer contribution accounts for 3% of overall spectral intensity. These results show that, astonishingly, hydrated DOPC bilayers remain intact and can accommodate up to 75 mol% (3:1) of BMA.

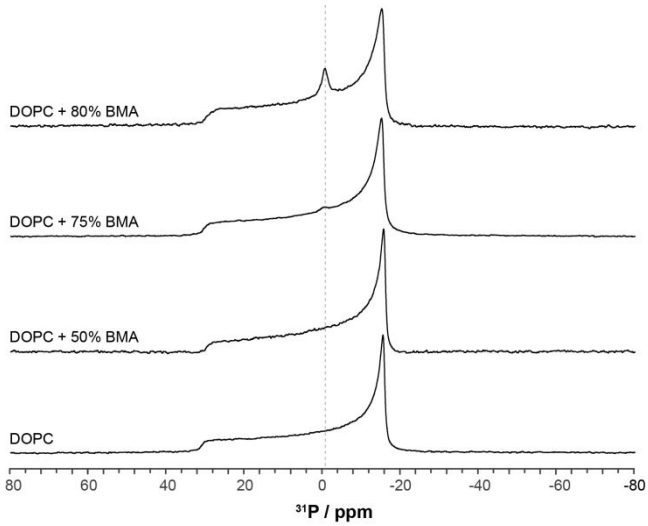

***Figure 2**. Wideline ^{31}P NMR spectra of hydrated DOPC MLVs alone (bottom) and with 50, 75 and 80% mol of BMA (top) acquired at 20°C. The dashed line guides the eye to the isotropic chemical shift for PC of -0.9 ppm, at which spectral contribution is observed from non-bilayer lipid assemblies present at high BMA levels.*

To investigate the role of lipid chain composition on membrane stability in the presence of 75 mol% BMA, we characterised a series of liposomes made of different hydrophobic chain length and saturation. The structures of each lipid molecule are shown in Figure 1. Short saturated 14-carbon chains reflect the fatty acid composition of lipid A, the membrane part of LPS found in the outer leaflet of bacterial outer membrane. Saturated 16-carbon chains and *cis*-unsaturated 18-carbon chains, as well as mixed 16-saturated/18-mono-unsaturated chains, have matching hydrophobic extension and are common constituents of plasma membrane lipids, as well as the inner leaflet of bacterial outer membranes. We also tested trans-unsaturated C18:1 elaidoylated lipids, which have been elevated in solvent-tolerant organisms[22,32].

Wideline ^{31}P NMR spectra of MLVs with different lipid composition alone and in the presence of 75 mol% BMA are shown in Figure 3. On the whole, all lipids remained in the bilayer phase at this high BMA concentration. Symmetric saturated 14-carbon chain, DMPC, showed slightly reduced stability in the presence of BMA in comparison to DOPC, POPC

and DEPC, as indicated by the small, isotropic peak observed around −1 ppm. DPPC, a 16-carbon saturated phospholipid with matching hydrophobic thickness to DOPC[43], also showed bilayers in coexistence with a small non-bilayer environment in BMA presence. Both di-saturated lipids showed a lower tolerance to BMA uptake in comparison to DOPC, which suggests that unsaturation is important for accommodating BMA into the membrane and for maintaining membrane integrity. Mixed chain POPC and di-*cis*-unsaturated DOPC showed similar and higher tolerance to BMA than saturated lipids, which shows that at least one unsaturated chain is sufficient for membranes.

In solvent-tolerant *Clostridia* enzymatic *cis*/*trans* isomerization has been associated with enhanced solvent tolerance. To gain insight into the comparative stability of such modified membranes we studied MLVs of DEPC alone and in the presence of 75 mol% BMA. The hydrophobic thickness of DEPC (trans-C18:1Δ9) matches saturated C18:0 in contrast to DOPC, which is matched to C16:0. The spectroscopic features of DEPC are dominated by a Pake pattern, shown in Figure 3, revealing a stable bilayer both without and with 75% BMA. While in the case of DOPC membranes we observed some small narrowing of the Pake pattern, consistent with subtle changes in rate and symmetry of fast molecular rotation, the DEPC ^{31}P spectra showed hardly any change in the presence of BMA, suggesting that the *trans* isomer is able to accommodate BMA even better than DOPC membranes with *cis* chains.

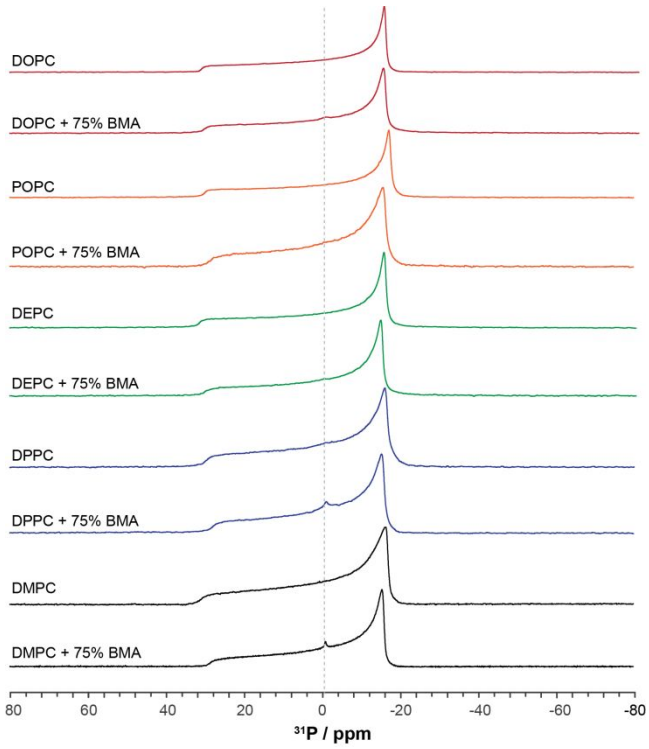

Figure 3. *Wideline ^{31}P NMR spectra of hydrated MLVs composed of (red) DOPC, (orange) POPC, (green) DEPC, (blue) DPPC and (black) DMPC, containing either (upper) no BMA and (lower) 75% mol of BMA. The spectra were recorded in the fluid* $\boldsymbol{L_\alpha}$ *phase at 20°C for DOPC, POPC and DEPC, 28°C for DMPC and 42°C for DPPC samples.*

Effects of BMA on lipid transition – ^{13}C MAS NMR

BMA is a relatively hydrophobic molecule with *Log P* = 2.88 and would likely partition into the hydrophobic membrane core. To confirm whether BMA is localised within the hydrophobic membrane core or whether it affects lipid phase behaviour *via* headgroup effects from the solvent, we used high resolution ^{13}C CP MAS NMR to observe BMA specifically embedded in membranes using natural abundance ^{13}C in membrane lipid and BMA. CP MAS efficiency is abolished in mobile molecular systems and the method can be used as a motion filter to select only motionally restricted, membrane-associated BMA while suppressing and BMA in solution. Figure 4 shows ^{13}C CP MAS spectra of DOPC, POPC, DEPC, DPPC and DMPC with 75 mol% BMA under 5 kHz MAS. The ^{13}C CP MAS spectra showed typical resolution of hydrated lipid bilayers[27]. Strong spectral contribution from BMA observed in all spectra clearly shows significant incorporation of BMA into all model membranes and while

CP in the strict sense is not quantitative, resonance intensity from BMA titration in lipid corresponds well to the actual stoichiometry in the system, as shown in Figure S2 of DMPC with 50%mol and 75%mol BMA incorporation. This suggests that the dynamics of membrane BMA and lipid occur on a similar timescale.

Lipid chain mobility is the main determinant of chain melting, which is reflected in the main transition temperature T_m between the liquid crystalline, L_α, and tilted lamellar gel phase, $P_{\beta'}$. The main transition temperature is determined by contributions from chain *trans-gauche* isomerisation and collective intermolecular chain-chain contacts[44] and is sensitive to modulation of these interaction that may result from incorporation of additional molecular species into the membrane interior or from changes in environmental factors, such as hydrostatic pressure.

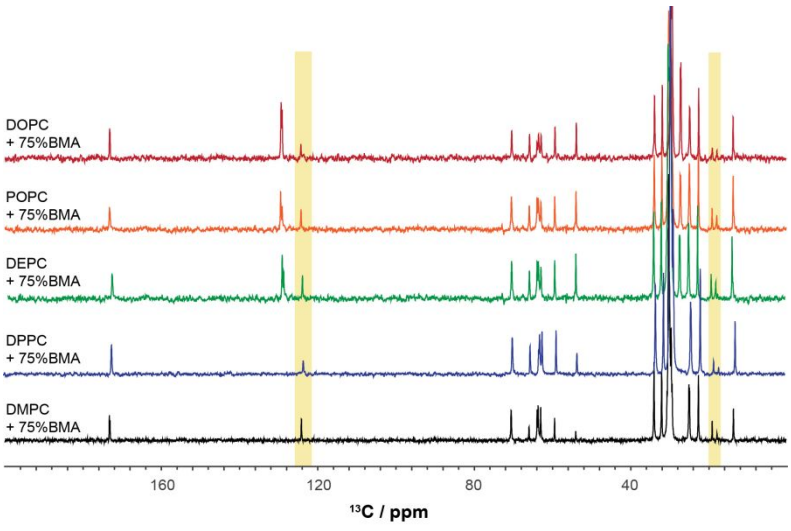

Figure 4. *^{13}C MAS CP NMR spectra of (red) DOPC, (orange) POPC, (green) DEPC, (blue) DPPC and (black) DMPC with 75% BMA spinning at 5 kHz, recorded using SPINAL decoupling during acquisition. The spectra were recorded in the fluid $\boldsymbol{L_\alpha}$ phase at 20°C for DOPC, POPC and DEPC, 28°C for DMPC and 42°C for DPPC samples. The yellow panels highlight characteristic resonances of BMA.*

High resolution J-resolved ^{13}C CP-MAS NMR under Lee-Goldburg decoupling is very

sensitive to changes in lipid segmental dynamics, reflected in the decoupling efficiency, and can be used to monitor changes in lipid transition temperature[37]. Figure 5(a) shows a series of J-resolved frequency-switched Lee-Goldburg, FSLG, decoupled ^{13}C MAS NMR spectra from hydrated DMPC membranes using natural abundance ^{13}C as reporter. Spectra acquired in the liquid crystalline phase (above 24°C) are characterised by well-resolved multiplets for each chemical environment with effective proximal J^{CH}-couplings scaled by $1/\sqrt{3}$ [32].

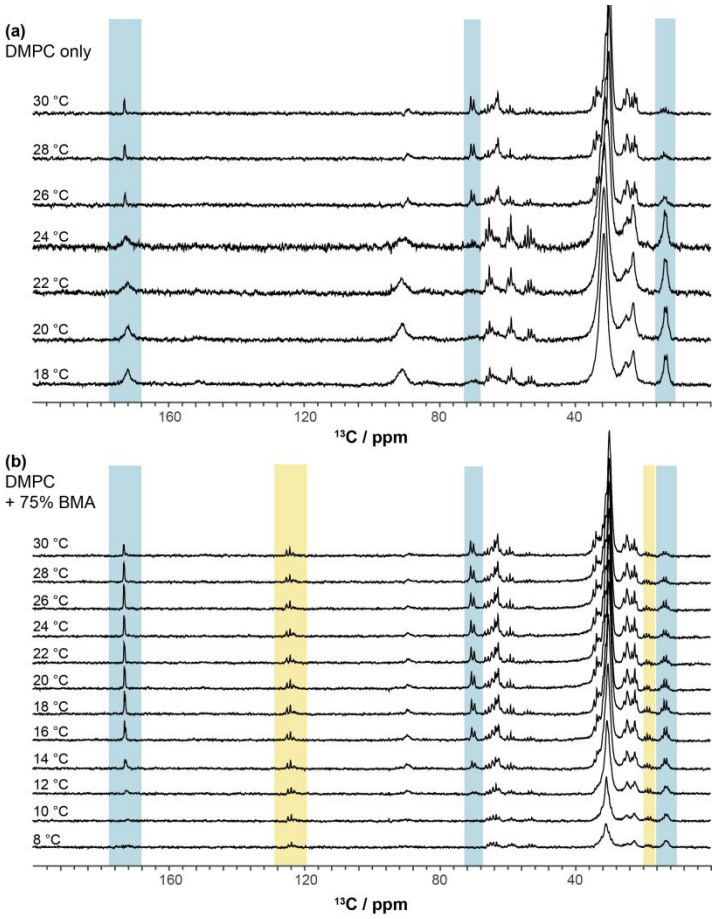

***Figure 5**. High resolution J resolved LG-CP ^{13}C MAS NMR spectra of hydrated DMPC MLVs without (a) and with 75% mol BMA (b) recorded at temperatures bracketing the 24˚C main transition in DMPC and the lower transition in the presence of BMA between 10 and 14˚C. Yellow highlights BMA signals, and blue highlights DMPC resonances used to determine the main transition temperature T_m.*

Below the main transition, lipid mobility slows down during collective freezing of lipid acyl chains and backbone, which enter slow/intermediate regime respectively, while headgroup dynamics remains fast. Marked spectral changes, include broadening of the carbonyl resonance at 173 ppm, loss of backbone intensity of glycerol sn-2 resonance at 70 ppm and loss of J-multiplet resolution in the acyl chains methyls at 14 ppm,

are used as indicators of phase transition from liquid crystalline to gel as the temperature lowered[37,38]. At the same time, headgroup resonances remain sharp and well-resolved. Motional restriction in the acyl chains is observed even above T_m for the terminal CH_3 in preparation for the transition[44]. Methyl intensity is comparatively enhanced in the $P_{\beta'}$ gel, as the rapid segmental dynamics that is dominant in the L_α phase is markedly attenuated, which improves CP transfer efficiency. As temperature decreases further and membranes enter the L_β phase (near 20°C), an increase in J-resolution is observed, which is associated with further stepwise enhancement in FSLG efficiency under slower segmental dynamics. Glycerol backbone *sn*-2' CH at 70 ppm showed a sharp doublet at temperature above T_m, while below T_m the resonance vanishes as a result of intermediate time scale motions. The carbonyl signal at 173 ppm shows a well-resolved peak above T_m, which diminishes near T_m and regains intensity in the gel greater resonance width (lower T_2^*).

In the presence of 75 mol% BMA, J-resolved ^{13}C CP MAS spectra from DMPC vesicles reveal a significant drop in transition temperature from 24°C to 12°C. Again, the *sn-2* glycerol backbone signal at 70 ppm and carbonyl signal at 173 ppm vanish at temperatures near T_m, which in this case is observed between 14 and 12°C in Figure 5(b). The transition is broader, due to phase co-existence in the two-component system. The decrease in T_m reflects lipid chain uncoupling and the breakdown of collective motions during lateral swelling of membrane to accommodate BMA molecules. Figure 6 shows the effect of BMA on DMPC phase transition temperature determined from ^{13}C MAS NMR. The decrease in DMPC T_m with increasing concentration of BMA suggests that BMA molecules intercalate between the

lipid chains and disrupt packing, while the bilayer structure is maintained. At high BMA level the comparative contribution from lipid chains is reduced and T_m is largely dominated by trans-gauche isomerisation.

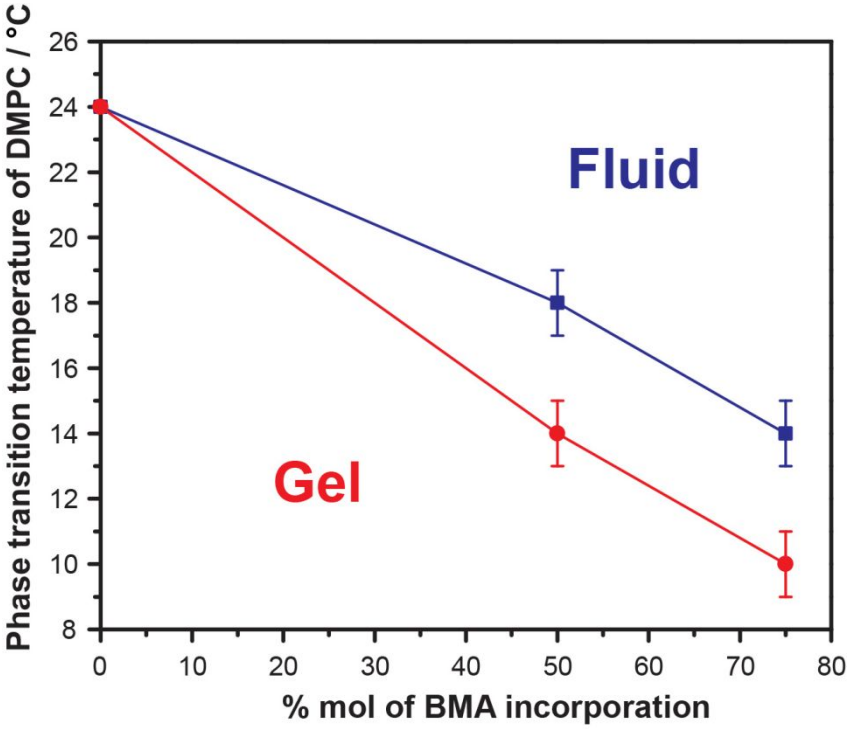

***Figure 6**. Outline of the hydrated DMPC/BMA phase diagram showing suppression of DMPC main chain melting transition temperature, T_m, determined from the LG-CP ^{13}C MAS NMR. The liquidus between the liquid crystal, $\boldsymbol{L_\alpha}$ phase and the two phase coexistence region is outlined in blue and the solidus between the two phase coexistence and the tilted gel phase, $\boldsymbol{L_{\beta'}}$, is shown in red*[44].

The presence of BMA signal at 125 ppm clearly shows its incorporation into the membrane, as Hartmann-Hahn transfer is only possible in immobile, membrane embedded molecular systems, but disrupted by rapid molecular tumbling fast in solution and not contributing to the CP spectra. Spectral features from BMA do not change across the lipid main transition, which suggests that BMA does neither participate in, nor mediate lipid collective motions and that the observed lower transition temperature T_m is determined largely by freezing the *trans-gauche* dynamics of the lipid chains.

Small angle X ray scattering

Small angle X-ray scattering, SAXS, offers a direct way of monitoring changes in the lamellar parameters from bilayer lipid membranes[28,45,46]. Besides vesicle size estimates[47,48], SAXS offers insights into bilayer thickness[28] and changes in the membrane interior[28]. We use SAXS from lipid suspensions to monitor changes in bilayer parameters in the presence of high concentrations of BMA.

Two possibilities arise when considering the membrane localisation of BMA at high BMA/lipid ratios: a) BMA could intercalate alongside and between lipid chains with preference for the carbonyl region; or, b) BMA could phase-separates between the leaflets and uncouple the two membrane leaflets. Observation of signal in the ^{13}C CP NMR spectra suggests the former mechanism, which would create a motionally restricted BMA environment observable by CP MAS NMR. While the NMR results reveal intercalation of BMA between the lipid acyl chains, we cannot rule out BMA accumulation between the two leaflets of the bilayer in addition to saturation of the acyl chain region based on NMR results alone. We employed SAXS to monitor possible changes in bilayer thickness or "swelling" of the bilayer and consequent uncoupling of the two leaflets in the presence of high amounts of BMA.

Hydrated MLV suspensions of DMPC, DOPC and DEPC with and without BMA were characterised by SAXS and the scattering profiles are shown in Figure 7. Well-resolved Bragg reflections are associated with the periodic bilayer repeat within the multilamellar

vesicles. The reflection at q = 0.1 Å^{-1} corresponds to first order reflection, at q = 0.2 Å^{-1} corresponds to n=2 and highly structured liposomes in the absence of BMA show a hint of a third order reflection[28]. We monitor the n=1 reflection as indicator of changes in lamellar periodicity on addition of BMA. Since neither PC nor BMA are charged, we expect the hydration layers to remain unaffected in the presence of BMA, which partitions with preference into the hydrophobic bilayer interior. Shown in Figure 7, the first Bragg peak is observed at slightly different q for DMPC, DOPC and DEPC, reflective of the increase in bilayer hydrophobic thickness in this order. This is seen in more detail in Figure S5 where the greatest hydrophobic thickness (C18:0-equivalent) DEPC showed q of 0.098 Å^{-1} corresponding to 64.1 Å bilayer repeat; DOPC and DMPC showed similar bilayer repeat with DOPC repeat of 62.8 Å and DMPC repeat of 61.9 Å, also showing slightly narrower reflections, consistent with higher number of stacked lamellae. The bilayer thickness was estimated using SAXS from LUVs and the scattering profiles showed bilayer thickness ranging from 26, 27 to 30 Å for DMPC, DOPC and DEPC, respectively, shown in Figure S6.

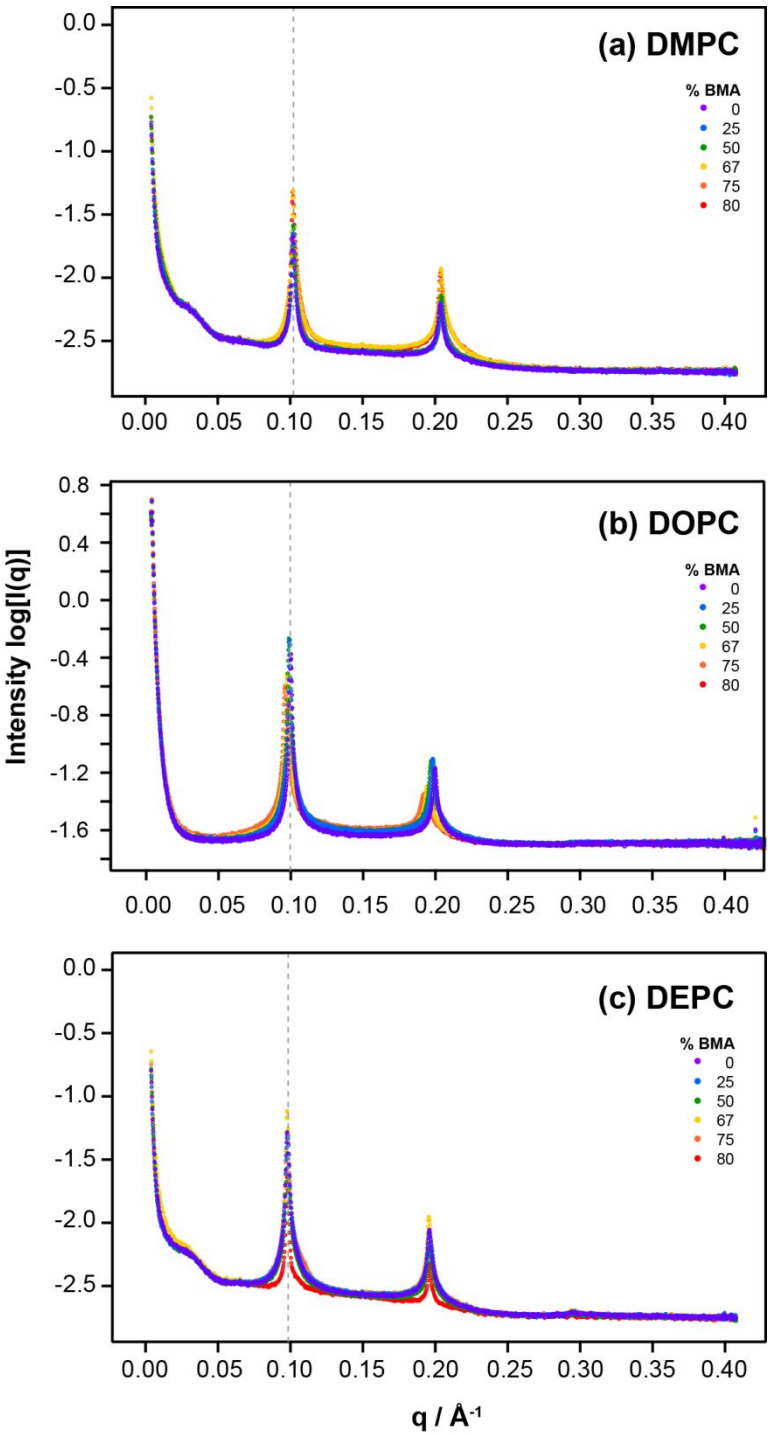

***Figure** 7. X-ray 1D scattering profiles from DMPC, DOPC and DEPC membranes in periodic MLV structures recorded at 30 °C, in the presence of BMA at 0, 25, 50, 67, 75 and 80% molar in hydrated (a) DMPC, (b) DOPC and (c) DEPC MLVs. The dotted lines mark the position of the first order reflections.*

Figures 7 show the SAXS results for vesicles composed of DMPC, DOPC and DEPC in the presence of different BMA molar ratios from 25% to 80 mol%. The Bragg reflections from each lipid appear to be independent of BMA concentration in the membrane, which confirms that as BMA incorporates into the membrane it does not affect membrane thickness and, therefore, accumulate between the lipid tails rather than forming a separate phase between the two membrane leaflets. The n=3 reflection at q = 0.3 Å^{-1} diminishes at higher BMA concentrations and disappears about 75 mol%. This corroborates the proposed

localisation of BMA between the chains and near the polar/apolar interface, as electron-dense BMA reduces headgroup/chain contrast at thigh concentrations.

A subtle variation in the Bragg reflections is observed for DOPC between 0 and 80 mol% BMA, where the bilayer repeat increases by approximately 2 Å as oleic chains assume a more extended average conformation under lateral pressure from BMA. This change is also seen in the MLV scattering profiles in Figure S6.

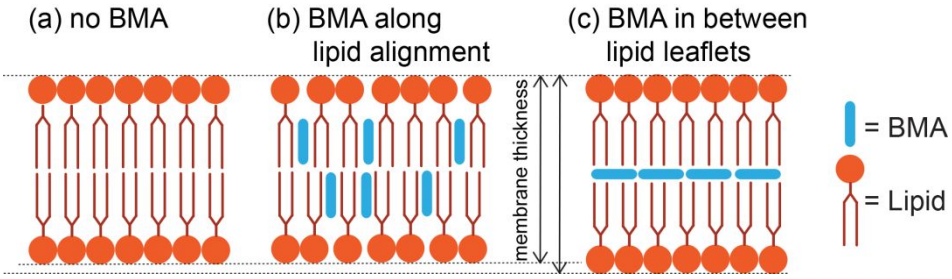

Figure 8. *Schematic of a lipid bilayer (a) and with putative BMA incorporation between the hydrocarbon chains (b) or as a separate subphase forming between the two leaflets of the membrane. Localization of BMA between the hydrocarbon chains (b) is substantiated by NMR and SAXS data, while BMA incorporation between the two leaflets (c) would result in increased membrane thickness, which is not observed in the SAXS.*

The SAXS results combined with the NMR findings reveal high levels of BMA insertion into lipid membranes with BMA intercalation between the lipid chains and molecules aligned alongside the hydrocarbon lipid chains, as shown in the schematic of Figure 8. Such BMA insertion causes lateral uncoupling of lipid chain dynamics without bilayer leaflet separation. Reduction in Bragg's intensity from hydrophobic repeats, observed with increasing BMA concentration, together with NMR data shows that BMA incorporates between the lipid

chains and penetrates the region near the hydrophobic-hydrophilic interface.

CONCLUSION

Recent development of industrial biotechnology mandates increased use of biorenewable non-food resources in place of petrochemicals to produce commodity chemicals and biofuels. Product toxicity during biofermentation, which currently limits process efficiency, has been related to membrane damage in the presence of high concentrations of apolar chemicals[7]. To understand better the mechanisms of toxicity, we investigated a series of model membranes with different hydrophobic chain composition – length, saturation and *cis*-*trans* isomerization state – in the presence of high, production-relevant concentrations of BMA. We observed that BMA partitions into bilayer lipid membranes, which can accommodate a surprisingly high levels of BMA, up to 75 mol% without losing bilayer integrity. The membrane tolerance to hydrophobic BMA is dependent on lipid chain composition with unsaturated chain lipids accommodating high amounts of BMA better than saturated chain lipids. Specifically, we found that *trans*-unsaturation show enhanced stability to BMA compared to *cis*-unsaturated chains, which corroborates reported biological response of microorganism in the presence of toluene[22].

Intercalation of BMA between the hydrophobic lipid chains resulted in significant depression of the chain melting temperature. Since transition temperature contains contributions from *trans*-*gauche* chain isomerization, as well as a collective contribution form intermolecular chain contact, at 3:1 and 4:1 BMA/lipid ratios we have successfully uncoupled interchain

contacts leaving the *trans-gauche* isomerisation as the leading determinant of the main transition. Saturation of the lipid region with BMA is corroborated by SAXS, where headgroup/chain contrast is diminished at high BMA concentrations. SAXS results also rule out the possibility of bilayer leaflet uncoupling by the formation of a separate BMA sub-phase, localised between the opposing acyl chains and swelling the membrane.

Membrane engineering studies have shown that altering membrane lipid chain length, saturation and composition can influence cell viability that may be beneficial to biofermentative manufacturing of hydrophobic solvents[49]. In particular, the conversion of *cis*- to *trans*-unsaturated fatty acids can increase solvent tolerance in *E. coli* and *P. putida* in a *Log P* dependent protective effect[6]. In this molecular study we corroborate this observation, reveal the impact of chain composition on membrane stability to solvents and demonstrate the importance of phospholipid chain composition as determinant of membrane tolerance to BMA.

ACKNOWLEDGEMENTS

The work was funded by the BBSRC IB-Catalyst grant BB/N010426/1 to BB. We like to thank Diamond Light Source for access to B21 beamline (SM16125 and SM21035-195). B21 beam-time on experimental line was granted by Diamond *via* rapid access route (http://www.diamond.ac.uk/Users.html).

ASSOCIATED CONTENT

Supporting information

Table S1: BMA to lipid ratio and their corresponding mol% alongside sample size;

Figure S1: Change in the appearance and buoyancy of centrifugated DOPC MLV samples after incorporation of 70 mol% BMA;

Figure S2: Carbon-13 CP MAS NMR spectra of DMPC with different amount of BMA;

Figure S3: Carbon-13 CP MAS NMR spectra of DMPC with and without BMA with different decoupling schemes;

Figure S4: Carbon-13 CP MAS NMR spectra of DMPC with 50% mol BMA at various temperature;

Figure S5: Normalised 1D X-ray scattering profiles of DMPC, DOPC and DEPC;

AUTHOR INFORMATION

Corresponding author: BB Email: boyan.bonev@nottingham.ac.uk

Author contributions: VY performed the NMR work, sample preparation and wrote the manuscript; AG was involved in the sample preparation and NMR and SAXS; GE was involved in the conceptual design, text edits and provided MAE; RR, KI and JD were involved in the SAXS experiments on Diamond B21 and text edits; BB was responsible for conceptual design, writing the manuscript and was involved in the NMR and SAXS experiments.

Funding: BBSRC IB Catalyst

Notes: none; Competing interest: none

REFERENCES

(1) Global Polymethyl Methacrylate Market (PMMA) - Industry Analysis and Forecast (2018-2026) https://www.maximizemarketresearch.com/market-report/global-polymethyl-methacrylate-market/26389/ (accessed Sep 19, 2019).

(2) Tang, W. L.; Zhao, H. Industrial Biotechnology: Tools and Applications. *Biotechnology Journal* 2009, *4* (12), 1725–1739.

(3) Soetaert, W.; Vandamme, E. The Impact of Industrial Biotechnology. *Biotechnology Journal* 2006, *1* (7–8), 756–769.

(4) Chen, C.; Ding, S.; Wang, D.; Li, Z.; Ye, Q. Simultaneous Saccharification and Fermentation of Cassava to Succinic Acid by Escherichia Coli NZN111. *Bioresource Technology* 2014, *163*, 100–105.

(5) Becker, J.; Lange, A.; Fabarius, J.; Wittmann, C. Top Value Platform Chemicals: Bio-Based Production of Organic Acids. *Current Opinion in Biotechnology* 2015, *36*, 168–175.

(6) Tan, Z.; Yoon, J. M.; Nielsen, D. R.; Shanks, J. V.; Jarboe, L. R. Membrane Engineering via Trans Unsaturated Fatty Acids Production Improves Escherichia Coli Robustness and Production of Biorenewables. *Metabolic Engineering* 2016, *35*, 105–113.

(7) Lennen, R. M.; Kruziki, M. A.; Kumar, K.; Zinkel, R. A.; Burnum, K. E.; Lipton, M. S.; Hoover, S. W.; Ranatunga, D. R.; Wittkopp, T. M.; Marner, W. D.; et al. Membrane Stresses Induced by Overproduction of Free Fatty Acids in Escherichia Coli. *Appl. Environ. Microbiol.* 2011, *77* (22), 8114–8128.

(8) Huffer, S.; Clark, M. E.; Ning, J. C.; Blanch, H. W.; Clark, D. S. Role of Alcohols in Growth, Lipid Composition, and Membrane Fluidity of Yeasts, Bacteria, and Archaea. *Appl. Environ. Microbiol.* 2011, *77* (18), 6400–6408.

(9) Sato, E.; Yu, F.; Mizunashi, W.; Nakajima, E. Method for Producing Methacrylic Acid Ester. EP2848694A1, March 18, 2015.

(10) Lanne, A. B. M.; Goode, A.; Prattley, C.; Kumari, D.; Drasbek, M. R.; Williams, P.; Conde-Álvarez, R.; Moriyón, I.; Bonev, B. B. Molecular Recognition of Lipopolysaccharide by the Lantibiotic Nisin. *Biochimica et Biophysica Acta (BBA) - Biomembranes* 2019, *1861* (1), 83–92.

(11) Morein, S.; Andersson, A.-S.; Rilfors, L.; Lindblom, G. Wild-Type Escherichia Coli

Cells Regulate the Membrane Lipid Composition in a Window between Gel and Non-Lamellar Structures. *J. Biol. Chem.* 1996, *271* (12), 6801–6809.

(12) Kaneda, T. Iso- and Anteiso-Fatty Acids in Bacteria: Biosynthesis, Function, and Taxonomic Significance. *Microbiology and Molecular Biology Reviews* 1991, *55* (2), 288–302.

(13) Sikkema, J.; de Bont, J. A.; Poolman, B. Mechanisms of Membrane Toxicity of Hydrocarbons. *Microbiol Rev* 1995, *59* (2), 201–222.

(14) Weber, F. J.; de Bont, J. A. M. Adaptation Mechanisms of Microorganisms to the Toxic Effects of Organic Solvents on Membranes. *Biochimica et Biophysica Acta (BBA) - Reviews on Biomembranes* 1996, *1286* (3), 225–245.

(15) Vermuë, M.; Sikkema, J.; Verheul, A.; Bakker, R.; Tramper, J. Toxicity of homologous series of organic solvents for the gram-positive bacteria Arthrobacter and Nocardia Sp. and the gram-negative bacteria Acinetobacter and Pseudomonas Sp. *Biotechnology and Bioengineering* 1993, *42* (6), 747–758.

(16) Inoue, A.; Horikoshi, K. Estimation of Solvent-Tolerance of Bacteria by the Solvent Parameter Log P. *Journal of Fermentation and Bioengineering* 1991, *71* (3), 194–196.

(17) Sullivan, K. H. Alteration of the Fatty Acid Composition of Escherichia Coli by Growth in the Presence of Normal Alcohols. *J. BACTERIOL.* 1979, *138*, 6.

(18) Ingram, L. O. Adaptation of Membrane Lipids to Alcohols. *Journal of Bacteriology* 1976, *125* (2), 670–678.

(19) Luzzati, V.; Husson, F. The Structure of the Liquid-Crystalline Phases of Lipid-Water Systems. *The Journal of Cell Biology* 1962, *12* (2), 207–219.

(20) De Smet, M. J.; Kingma, J.; Witholt, B. The Effect of Toluene on the Structure and Permeability of the Outer and Cytoplasmic Membranes of Escherichia Coli. *Biochimica et Biophysica Acta (BBA) - Biomembranes* 1978, *506* (1), 64–80.

(21) Inoue, A.; Horikoshi, K. A Pseudomonas Thrives in High Concentrations of Toluene. *Nature* 1989, *338* (6212), 264–266.

(22) Heipieper, H. J.; Weber, F. J.; Sikkema, J.; Keweloh, H.; de Bont, J. A. M. Mechanisms of Resistance of Whole Cells to Toxic Organic Solvents. *Trends in Biotechnology* 1994, *12* (10), 409–415.

(23) Hansch, C.; Leo, A.; Hoekman, D. H. *Exploring QSAR.: Hydrophobic, Electronic, and Steric Constants*; American Chemical Society, 1995.

(24) Penzel, E.; Ballard, N.; Asua, J. M. Polyacrylates. In *Ullmann's Encyclopedia of*

Industrial Chemistry; Wiley-VCH Verlag GmbH & Co. KGaA: Weinheim, Germany, 2018; pp 1–20.

(25) Bonev, B.; Watts, A.; Bokvist, M.; Gröbner, G. Electrostatic Peptide–Lipid Interactions of Amyloid-β Peptide and Pentalysine with Membrane Surfaces Monitored by 31P MAS NMR. *Physical Chemistry Chemical Physics* 2001, *3* (14), 2904–2910.

(26) Bonev, B. B.; Lam, Y.-H.; Anderluh, G.; Watts, A.; Norton, R. S.; Separovic, F. Effects of the Eukaryotic Pore-Forming Cytolysin Equinatoxin II on Lipid Membranes and the Role of Sphingomyelin. *Biophysical Journal* 2003, *84* (4), 2382–2392.

(27) Drechsler, A.; Separovic, F. Solid-State NMR Structure Determination. *IUBMB Life (International Union of Biochemistry and Molecular Biology: Life)* 2003, *55* (9), 515–523.

(28) Nagle, J. F.; Tristram-Nagle, S. Structure of Lipid Bilayers. *Biochimica et Biophysica Acta (BBA) - Reviews on Biomembranes* 2000, *1469* (3), 159–195.

(29) Eliasz, A. W.; Chapman, D.; Ewing, D. F. Phospholipid Phase Transitions. Effects of n-Alcohols, n-Monocarboxylic Acids, Phenylalkyl Alcohols and Quatenary Ammonium Compounds. *Biochimica et Biophysica Acta (BBA) - Biomembranes* 1976, *448* (2), 220–233.

(30) Ramos, J. L.; Duque, E.; Rodríguez-Herva, J.-J.; Godoy, P.; Haïdour, A.; Reyes, F.; Fernández-Barrero, A. Mechanisms for Solvent Tolerance in Bacteria. *J. Biol. Chem.* 1997, *272* (7), 3887–3890.

(31) Sardessai, Y.; Bhosle, S. Tolerance of Bacteria to Organic Solvents. *Research in Microbiology* 2002, *153* (5), 263–268.

(32) Heipieper, H. J.; Bont, J. A. de. Adaptation of Pseudomonas Putida S12 to Ethanol and Toluene at the Level of Fatty Acid Composition of Membranes. *Appl. Environ. Microbiol.* 1994, *60* (12), 4440–4444.

(33) Pinkart, H. C.; Wolfram, J. W.; Rogers, R.; White, D. C. Cell Envelope Changes in Solvent-Tolerant and Solvent-Sensitive Pseudomonas Putida Strains Following Exposure to o-Xylene. *Appl. Environ. Microbiol.* 1996, *62* (3), 1129–1132.

(34) Dombek, K. M.; Ingram, L. O. Effects of Ethanol on the Escherichia Coli Plasma Membrane. *Journal of Bacteriology* 1984, *157* (1), 233–239.

(35) Kobayashi, H.; Yamamoto, M.; Aono, R. Appearance of a Stress-Response Protein, Phage-Shock Protein A, in Escherichia Coli Exposed to Hydrophobic Organic Solvents.

Microbiology 1998, *144* (2), 353–359.

(36) Parisot, J.; Carey, S.; Breukink, E.; Chan, W. C.; Narbad, A.; Bonev, B. Molecular Mechanism of Target Recognition by Subtilin, a Class I Lanthionine Antibiotic. *Antimicrobial Agents and Chemotherapy* 2008, *52* (2), 612–618.

(37) Ciesielski, F.; Griffin, D. C.; Rittig, M.; Bonev, B. B. High-Resolution J-Coupled 13C MAS NMR Spectroscopy of Lipid Membranes. *Chemistry and Physics of Lipids* 2009, *161* (2), 77–85.

(38) Zorin, V.; Ciesielski, F.; Griffin, D. C.; Rittig, M.; Bonev, B. B. Heteronuclear Chemical Shift Correlation and J-Resolved MAS NMR Spectroscopy of Lipid Membranes. *Magnetic Resonance in Chemistry* 2010, *48* (12), 925–934.

(39) Fung, B. M.; Khitrin, A. K.; Ermolaev, K. An Improved Broadband Decoupling Sequence for Liquid Crystals and Solids. *Journal of Magnetic Resonance* 2000, *142* (1), 97–101.

(40) Lee, M.; Goldburg, W. I. Nuclear-Magnetic-Resonance Line Narrowing by a Rotating Rf Field. *Phys. Rev.* 1965, *140* (4A), A1261–A1271.

(41) Bonev, B. B. High-Resolution Solid-State NMR of Lipid Membranes. In *Advances in Planar Lipid Bilayers and Liposomes*; Elsevier, 2013; Vol. 17, pp 299–329.

(42) Ulrich, A. S.; Sami, M.; Watts, A. Hydration of DOPC Bilayers by Differential Scanning Calorimetry. *Biochimica et Biophysica Acta (BBA) - Biomembranes* 1994, *1191* (1), 225–230.

(43) Sani, M.-A.; Whitwell, T. C.; Separovic, F. Lipid Composition Regulates the Conformation and Insertion of the Antimicrobial Peptide Maculatin 1.1. *Biochimica et Biophysica Acta (BBA) - Biomembranes* 2012, *1818* (2), 205–211.

(44) Bonev, B. B.; Morrow, M. R. Effect of Pressure on the Dimyristoylphosphatidylcholine Bilayer Main Transition. *Physical Review E* 1997, *55* (5), 5825–5833.

(45) Fogarty, J. C.; Arjunwadkar, M.; Pandit, S. A.; Pan, J. Atomically Detailed Lipid Bilayer Models for the Interpretation of Small Angle Neutron and X-Ray Scattering Data. *Biochimica et Biophysica Acta (BBA) - Biomembranes* 2015, *1848* (2), 662–672.

(46) Pabst, G.; Kučerka, N.; Nieh, M.-P.; Rheinstädter, M. C.; Katsaras, J. Applications of Neutron and X-Ray Scattering to the Study of Biologically Relevant Model Membranes. *Chemistry and Physics of Lipids* 2010, *163* (6), 460–479.

(47) Garcia-Diez, R.; Gollwitzer, C.; Krumrey, M.; Varga, Z. Size Determination of a

Liposomal Drug by Small-Angle X-Ray Scattering Using Continuous Contrast Variation. *Langmuir* 2016, *32* (3), 772–778.

(48) Jousma, H.; Talsma, H.; Spies, F.; Joosten, J. G. H.; Junginger, H. E.; Crommelin, D. J. A. Characterization of Liposomes. The Influence of Extrusion of Multilamellar Vesicles through Polycarbonate Membranes on Particle Size, Particle Size Distribution and Number of Bilayers. *International Journal of Pharmaceutics* 1987, *35* (3), 263–274.

(49) Lennen, R. M.; Pfleger, B. F. Modulating Membrane Composition Alters Free Fatty Acid Tolerance in Escherichia Coli. *PLOS ONE* 2013, *8* (1), e54031.

Figure captions

Figure 1. Chemical structures of DOPC, POPC, DEPC, DPPC and DMPC showing differences in the lipid chains alongside the structure of BMA.

Figure 2. Wideline ^{31}P NMR spectra of hydrated DOPC MLVs alone (bottom) and with 50, 75 and 80% mol of BMA (top) acquired at 20°C. The dashed line guides the eye to the isotropic chemical shift for PC of -0.9 ppm, at which spectral contribution is observed from non-bilayer lipid assemblies present at high BMA levels.

Figure 3. Wideline ^{31}P NMR spectra of hydrated MLVs composed of (red) DOPC, (orange) POPC, (green) DEPC, (blue) DPPC and (black) DMPC, containing either (upper) no BMA and (lower) 75% mol of BMA. The spectra were recorded in the fluid $\boldsymbol{L_\alpha}$ phase at 20°C for DOPC, POPC and DEPC, 28°C for DMPC and 42°C for DPPC samples.

Figure 4. ^{13}C MAS CP NMR spectra of (red) DOPC, (orange) POPC, (green) DEPC, (blue) DPPC and (black) DMPC with 75% BMA spinning at 5 kHz, recorded using SPINAL decoupling during acquisition. The spectra were recorded in the fluid $\mathbf{L_\alpha}$ phase at 20°C for DOPC, POPC and DEPC, 28°C for DMPC and 42°C for DPPC samples. The yellow panels highlight characteristic resonances of BMA.

Figure 5. High resolution J resolved LG-CP ^{13}C MAS NMR spectra [Ciesielski et al., Chem Phys Lipids 2009] of hydrated DMPC MLVs without (a) and with 75% mol BMA (b) recorded at temperatures bracketing the 24˚C main transition in DMPC and the lower transition in the presence of BMA between 10 and 14˚C. Yellow highlights BMA signals, and blue highlights DMPC resonances used to determine the main transition temperature T_m.

Figure 6. Outline of the hydrated DMPC/BMA phase diagram showing suppression of DMPC main chain melting transition temperature, T_m, determined from the LG-CP ^{13}C MAS NMR. The *liquidus* between the liquid crystal, $\boldsymbol{L_\alpha}$, phase and the tow phase coexistence region is outlined in blue and the *solidus* between the two phase coexistence and the tilted gel phase, $\boldsymbol{L_{\beta'}}$, is shown in red [Bonev&Morrow, Phys Rev E 1997].

Figure 7. X-ray 1D scattering profiles from DMPC, DOPC and DEPC membranes in periodic MLV structures recorded at 30 °C, in the presence of BMA at 0, 25, 50, 67, 75 and 80% molar in hydrated (a) DMPC, (b) DOPC and (c) DEPC MLVs.

Figure 8. Schematic of a lipid bilayer (a) and with putative BMA incorporation between the hydrocarpon chains (b) or as a separate subphase forming between the two leaflets of the membrane. Localization of BMA between the hydrocarbon chains (b) is substantiated by NMR and SAXS data, while BMA incorporation between the two leaflets (c) would result in

increased membrane thickness, which is not observed in the SAXS.

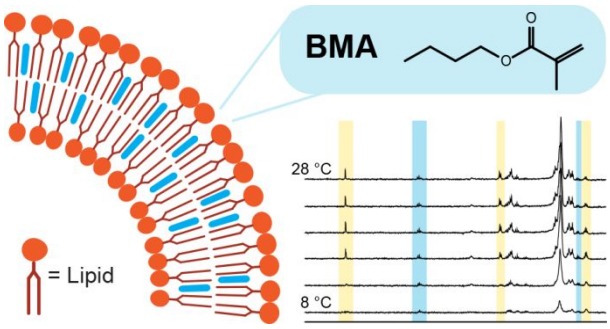

For Table of Contents Use Only